ChemPubSoc Europe

DOI: 10.1002/chem.201502154

CHEMISTRY A European Journal Full Paper

Anticancer Compounds |*Hot Paper*|

Cyclometalated Ruthenium(II) Anthraquinone Complexes Exhibit Strong Anticancer Activity in Hypoxic Tumor Cells

Leli Zeng, Yu Chen, Huaiyi Huang, Jinquan Wang, Donglei Zhao, Liangnian Ji, and Hui Chao*[a]

Abstract: Hypoxia is the critical feature of the tumor microenvironment that is known to lead to resistance to many chemotherapeutic drugs. Six novel ruthenium(II) anthraquinone complexes were designed and synthesized; they exhibit similar or superior cytotoxicity compared to cisplatin in hypoxic HeLa, A549, and multidrug-resistant (A549R) tumor cell lines. Their anticancer activities are related to their lipophilicity and cellular uptake; therefore, these physicochemical properties of the complexes can be changed by modifying the ligands to obtain better anticancer candidates. Complex **1**, the most potent member of the series, is highly active against hypoxic HeLa cancer cells ($IC_{50} = 0.53$ μM). This complex likely has 46-fold better activity than cisplatin ($IC_{50} = 24.62$ μM) in HeLa cells. This complex tends to accumulate in the mitochondria and the nucleus of hypoxic HeLa cells. Further mechanistic studies show that complex **1** induced cell apoptosis during hypoxia through multiple pathways, including those of DNA damage, mitochondrial dysfunction, and the inhibition of DNA replication and HIF-1α expression, making it an outstanding candidate for further in vivo studies.

Introduction

Hypoxia is related to the resistance of cancer cells to radiotherapy and chemotherapy.[1] In particular, the low oxygen levels (hypoxia), which are one of the critical features of the solid tumor environment, have received more attention.[2] As we know, oxygen is a key metabolite and oxygen homeostasis is important to human cancer cell survival. However, the available oxygen is consumed by the rapid and uncontrolled cancer cell proliferation; therefore, only a limited amount of oxygen is available to diffuse deep into the tumor tissue.[3] In addition, a low vessel density is considered as a marker of hypoxia. These vessels are abnormal and have impaired functions,[4] which handicap the delivery of sufficient oxygen and materials to the hypoxic tumor cells. Therefore, the drug cannot be effectively delivered to kill these hypoxic tumor cells.[5] On the other hand, reports on tumor hypoxia suggest that hypoxic adaptation should be considered in the management of solid tumors by adjusting the physiological activities of the tumor cells.[6] Hypoxia has a significant influence on intracellular physiological activities, such as cell proliferation, cell cycle progression, apoptosis, cell uptake, and others.[7] More than eighty genes associated with these tumor physiological activities are up-regulated in hypoxia through the transcriptional activity of the heterodimeric transcription factor, that is, the hypoxia inducible factor (HIF-1).[8] Currently, HIF-1 inhibition is an important strategy for cancer therapy.[9] Research on the efficacy of cancer drugs is usually performed in normoxia, which may not be a true indicator of cancer treatment effectiveness. Therefore, it is important to test anticancer drugs in hypoxic tumor cells.

Tumor tissues are hypoxic and show an overexpression of quinone oxidoreductase compared to normal tissues,[10] which is known to activate quinone-bearing anticancer drugs. Anthraquinone complexes,[11] such as ametantrone (AT), doxorubicin, emodin, and mitoxantrone (MX), demonstrate potent antitumor activity and have been extensively used in the clinic since the 1980s.[12] Anthraquinone compounds have been reported to be good candidates with multiple target molecules, and they generally act as intercalators or inhibit telomerase, DNA topoisomerase, HIF-1α, and some biomarkers.[13] The design of next-generation drugs with multiple targets and moieties with synergistic potency improves the activities and efficacy of the drugs.[14] However, most of these complexes are organic molecules, and their low solubility in water limits their further application. Currently, organometallic complexes with properties that are somewhat intermediate between the classical inorganic and organic molecules have recently been considered as promising alternatives.[15] Moreover, our group has designed polypyridyl ruthenium(II) complexes, containing anthraquinone ligands as anticancer drugs, and they exhibited some anticancer activity.[16] We have continued the research to improve the anticancer activity and selectivity of these complexes. Notably, Pfeffer et al. and our group have recently found that cyclome-

[a] *L. Zeng, Dr. Y. Chen, H. Huang, J. Wang, D. Zhao, Prof. L. Ji, Prof. Dr. H. Chao*
MOE Key Laboratory of Bioinorganic and Synthetic Chemistry
School of Chemistry and Chemical Engineering, Sun Yat-Sen University
Guangzhou 510275 (P. R. China)
E-mail: ceschh@mail.sysu.edu.cn

Supporting information for this article is available on the WWW under http://dx.doi.org/10.1002/chem.201502154.

talation can greatly increase the anticancer activity of the complexes,[17] which inspired us to integrate anthraquinones with cyclometalation to develop a novel series of tridentate ruthenium(II) anticancer drugs. These complexes enjoy a wide range of advantages:

1) These bistridentate Ru^{II} complexes could avoid geometrical isomers that may have different activity and selectivity against cancer cells.
2) Cyclometalation greatly increased the cellular uptake and toxicity of the Ru^{II} complexes.
3) The use of the anthracene-9,10-dione groups as a functional ligand could increase the interaction and activity of the Ru^{II} complexes with biomolecules.

Here, we synthesized and characterized six novel bistridentate ruthenium(II) complexes with anthraquinone substituents as functional ligands (Scheme 1, Figures S1–S15 in the Supporting Information). They were grouped into C,N,N-cyclometalated and N,N,N-non-cyclometalated Ru^{II} complexes. In this work, we studied the changes in the biological activity and physicochemical properties due to the modifications of the structure of the Ru^{II} complexes. The anticancer activity of the complexes was investigated in both 2D monolayer cells (normoxia/hypoxia) and 3D multicellular tumor spheroids.[18] Complex **1** can successfully exhibit potent in vitro cytotoxicity that is higher than cisplatin and the other five Ru^{II} complexes against all of the cancer cells screened. Further mechanistic studies in hypoxia show that complex **1** can efficiently induce apoptosis in HeLa cells through DNA damage, mitochondrial dysfunction, and the inhibition of DNA replication and HIF-1α expression.

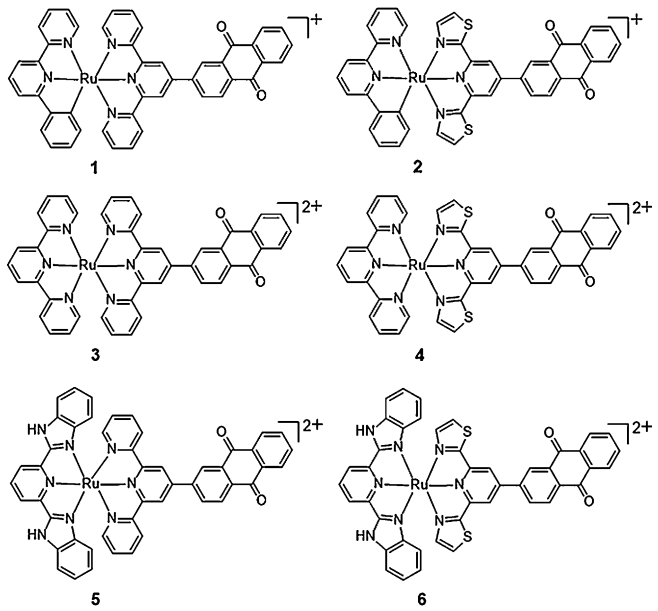

Scheme 1. Chemical structures of the Ru^{II} complexes **1**–**6**.

Results and Discussion

Synthesis and characterization

The ligands 2-([2,2′:6′,2″-terpyridin]-4′-yl)anthracene-9,10-dione (adtpy) and 2-(2,6-di(thiazol-2-yl)pyridin-4-yl)anthracene-9,10-dione (addpy) were prepared according to previously described procedures,[19] as illustrated in Figure S1 in the Supporting Information. The complexes [Ru(pbpy)(adtpy)](ClO_4) (**1**) (pbpy = 6-phenyl-2,2′-bipyridine) and [Ru(pbpy)(addtpy)](ClO_4) (**2**) were synthesized by heating Ru(adtpy)Cl_3/Ru(addpy)Cl_3 and AgOTf (Tf = triflate) to reflux in an acetone solution for 3 h. Then, 6-phenyl-2,2′-bipyridine was added to the residue and the mixture was heated to reflux in DMF under an argon atmosphere for 24 h. After adding a saturated aqueous solution of $NaClO_4$, a dark purple precipitate was collected and purified by alumina column chromatography with acetonitrile/toluene (1:1 to 10:1, v/v) as the eluent.[20] The complexes [Ru(tpy)(adtpy)](ClO_4)$_2$ (**3**) (tpy = 2,2′:6′,2″-terpyridine), [Ru(tpy)(addpy)](ClO_4)$_2$ (**4**), [Ru(bbp)(adtpy)](ClO_4)$_2$ (**5**) (bbp = 2,6-bis(benzimidazol-2-yl)pyridine), and [Ru(bbp)(addpy)](ClO_4)$_2$ (**6**) were synthesized by heating Ru(adtpy)Cl_3/Ru(addpy)Cl_3 and one equivalent of 2,2′:6′,2″-terpyridine or 2,6-bis(benzimidazol-2-yl)pyridine, respectively, to reflux in 70% aqueous ethanol for 12 h, followed by anion exchange with $NaClO_4$, purification by alumina flash column chromatography, and elution with acetonitrile/toluene (5:1, v/v). Complexes **1**–**6** were characterized by IR and ^{1}H NMR spectroscopy as well as ESI mass spectrometry and elemental analysis. In the infrared spectra, these complexes show characteristic absorption peaks at approximately $\tilde{\nu} = 1680\ cm^{-1}$, which suggests that they contain the C=O substituent.[13c] In addition, only a monocationic signal of $[M-ClO_4]^+$ was detected in the ESI spectra of complexes **1** and **2** (Figures S2 and S3 in the Supporting Information); however, in the non-cyclometalated complexes **3**, **4**, **5**, and **6**, the signals for $[M-2ClO_4-H]^+$ and $[M-2ClO_4]^{2+}$ were observed (Figures S4–S7 in the Supporting Information). Importantly, in ^{1}H NMR spectroscopy, the cyclometalated and non-cyclometalated complexes have an intrinsic variation on the proton in *ortho* or *para* position to the C_{aryl} atom bound to the Ru center.[21] For example, the chemical shift of the proton in *ortho* position to the C_{aryl} atom, which bounds to the Ru center, in complex **1** at $\delta = 5.66$ ppm is shifted upfield by 1.6 ppm compared to the similar proton in complex **3**, which was found at $\delta = 7.26$ ppm (Figures S10 and S12 in the Supporting Information).[20] Such shifts are primarily ascribed to the binding of the anionic cyclometalating ligand with the Ru metal, which causes an increase in the electron density at the Ru metal center and a decrease in the positive charge of the Ru metal center compared to the neutral non-cyclometalated ligands. These shifts are the origin of the differences in the biological activity for these Ru^{II} complexes.

Octanol/water partition coefficients

Octanol/water partition coefficients ($\log P_{o/w}$) provide a measure of the drug lipophilicity, which indicates the ability of the mol-

Table 1. IC_{50} values of the complexes towards different cell lines[a] in normoxia (20% O_2), hypoxia (1% O_2), and MCTSs.[b]

Complexes	HeLa			A549		A549R		L02
	normoxia	hypoxia	MCTSs	normoxia	hypoxia	normoxia	hypoxia	normoxia
1	(0.51 ± 0.05)	(0.53 ± 0.03)	(1.05 ± 0.13)	(0.55 ± 0.10)	(0.61 ± 0.85)	(0.57 ± 1.23)	(0.60 ± 0.68)	(4.50 ± 0.35)
2	(1.05 ± 0.21)	(1.68 ± 0.15)	(3.26 ± 0.31)	(1.39 ± 0.21)	(1.86 ± 0.10)	(2.31 ± 0.16)	(2.54 ± 0.33)	(5.01 ± 0.41)
3	(96.61 ± 5.6)	(110.4 ± 10.1)	> 200	(106.52 ± 4.7)	(110.5 ± 8.05)	(105.75 ± 6.22)	(115.6 ± 10.37)	(118.7 ± 6.07)
4	(105.65 ± 5.37)	(122.6 ± 8.63)	> 200	(112.5 ± 6.72)	(121.4 ± 4.57)	(113.65 ± 4.33)	(123.8 ± 8.62)	(129.5 ± 10.8)
5	(18.35 ± 2.0)	(22.21 ± 2.43)	(52.25 ± 3.30)	(25.90 ± 2.40)	(27.56 ± 3.06)	(21.67 ± 1.46)	(25.50 ± 1.65)	(27.11 ± 2.30)
6	(22.46 ± 3.45)	(26.56 ± 1.65)	(60.45 ± 1.64)	(24.76 ± 2.31)	(30.70 ± 2.53)	(27.52 ± 2.04)	(29.64 ± 1.57)	(30.22 ± 1.63)
cisplatin	(21.50 ± 1.60)	(24.62 ± 1.24)	(64.63 ± 2.70)	(22.35 ± 3.18)	(26.31 ± 2.23)	(135.36 ± 11.36)	(150.0 ± 10.64)	(18.76 ± 1.07)

[a] Cells were treated with various concentrations of the tested complexes for 48 h. [b] MCTSs (≈400 μm in diameter) were treated with various concentrations of the tested complexes for 48 h. Each value represents the mean ± SD of three independent experiments.

ecule to pass through cell membranes. The cyclometalated Ru^{II} complexes **1** and **2** are more hydrophobic than the non-cyclometalated Ru^{II} complexes **3**–**6** (Figure S16 in the Supporting Information). Complexes **3** and **4** gave negative $\log P_{o/w}$ values, suggesting that they are hydrophilic in nature. In contrast, complex **1** exhibited the highest $\log P_{o/w}$ value, indicating that this complex is the most hydrophobic. Complexes **2**, **5**, and **6** were proven to be moderately hydrophobic due to their positive $\log P_{o/w}$ values.

Cytotoxicity in normoxic and hypoxic 2D cancer cell cultures

The six new complexes were evaluated against three tumor cell lines derived from different tissues, including the cervix (HeLa), lung (A549), and cisplatin-resistant A549 cells (A549R). For comparison, the cisplatin cytotoxicity was also evaluated. As a control, the toxicity of the complexes was also tested against the normal L02 human cell line. Table 1 shows the IC_{50} values of the six complexes after a 48 h incubation as determined by a 3-(4,5-dimethylthiazol-2-yl)-2,5-diphenyltetrazolium bromide (MTT) assay. Based on the IC_{50} values, the in vitro antiproliferative efficacies of the complexes are in the following order: **1** > **2** > cisplatin ≈ **5** > **6** > **3** > **4**. Remarkable differences were observed that exceeded our expectations, with the cyclometalated complexes **1** and **2** exhibiting much higher cytotoxicity (IC_{50} values ranged from 0.51 to 2.54 μM) toward the entire cancer cell lines tested than the non-cyclometalated complexes **3** and **4**, which were almost non-toxic (IC_{50} values were all above 100 μM). In addition, complexes **5** and **6** exhibited a moderate cytotoxicity against the cancer cell lines. Complex **1** displayed an IC_{50} value (0.51 μM) that was over 200-fold lower than that of complex **4** (105.65 μM) against the HeLa human cervical cancer cell line. Complex **1** exhibited IC_{50} values approximately one order of magnitude lower than the ones of cisplatin under the same conditions. Complex **1** was also active against the cisplatin-resistant A549R cell line, with an IC_{50} value of 0.57 μM compared to 135.36 μM for cisplatin (a 264-fold difference). Most importantly, complex **1** was less cytotoxic to the normal L02 cell line (4.5 μM) than the cancer cell lines, thereby indicating improved selectivity for cancer cells.

A hypoxic region will occur when cells obtain an insufficient supply of oxygen. Tumors can increase their resistance to radiotherapy and many chemotherapies in hypoxia.[22] In addition, tumor hypoxia can profoundly affect the malignant progression of cancerous cells.[23] We further discussed the sensitivity of the cancer cell lines to the six complexes during hypoxia (1% O_2). Excitingly, the cytotoxicity of the six complexes for the cancer cell lines in hypoxia is similar to that in normoxia (Table 1). For instance, the IC_{50} value of complex **1** was approximately 0.53 μM for HeLa cells, 0.61 μM for A549 cells, and 0.60 μM for A549R cells in hypoxia, indicating that complex **1** is also active in the hypoxic tumor cells. In addition, the concentration-dependent cell-killing kinetics of complex **1** are depicted through a real-time cell growth assay.[24] As shown in Figure S17 in the Supporting Information, untreated HeLa cells grow normally and no distinct difference was observed between normoxia and hypoxia. However, with the doses of complex **1** (1.0 μM) experience rapidly abolished cellular proliferation in both normoxia and hypoxia, which indicated that HeLa cells undergo non-reversible senescence. The observation in real-time monitoring agrees with the cytotoxicity data described above.

Toxicity in 3D multicellular tumor spheroids (MCTSs)

Compared to 2D cultures, tumor cells in spheroids show an increased and more reproducible concentric arrangement of different cell populations. Moreover, the extracellular matrix is an inherent property of solid tumors,[25] which contributes to the increased multidrug resistance (MDR) in solid tumors.[26] Hence, a 3D model, or MCTS, is introduced to mimic the solid tumor in vitro and to study the viability of tumors treated with the Ru^{II} complexes.[27] The physiological state of the spheroids clearly depends on the spheroid size, and a hypoxic environment is generated in the center of the tumor. Spheroids with diameters up to 400 μm are frequently cultured for drug testing.[28] The MCTSs (400 μm) were treated with the Ru^{II} complexes and cisplatin. Similar to the 2D cell models, complexes **3** and **4** show slight toxicity to the MCTSs at a concentration of 100 μM with a 48 h incubation, and complexes **5** and **6** show moderate inhibition of the MCTSs at a concentration of 30.0 μM. However, the cyclometalated complexes **1** and **2** can exhibit a cytotoxic effect on the MCTSs at a concentration of 1.0 μM (Figures 1a and b). As shown in Table 1, the IC_{50} value of complex **1** on 400 μm MCTSs is 1.05 μM, which was 61-fold and 3.1-fold lower than cisplatin and complex **2**, respectively,

and far less than that of the four non-cyclometalated complexes. The size of the MCTSs treated with various concentrations of the complexes is exhibited in Figures 1a and b. The MCTSs treated with complex **1** are the smallest compared to the MCTSs treated with the other complexes under the same condition, indicating that complex **1** has the best anti-proliferative activity against HeLa cell spheroids.

The viability of the complex-treated MCTSs was also confirmed by using fluorescence microscopy and the live/dead cell assay,[29] a calcein AM and EthD-1 dual staining assay. Live cells stained with calcein AM yield a green fluorescence signal, whereas dead cells exhibit a red signal due to the EthD-1. As shown in Figure 1c, untreated living MCTSs and MCTSs treated with the Ru^{II} complexes (**3**, **4**, **5**, and **6**, 15.0 μM) and cisplatin (15.0 μM) emitted strong green fluorescence, which indicated that most of the cancer cells in the MCTSs were alive. However, the MCTSs treated with 2.0 μM of the cyclometalated complexes **1** and **2** and cisplatin (60.0 μM) showed weak green fluorescence and emitted strong red fluorescence, which suggested that complexes **1** and **2** induced cell death. The observation in the live/dead cell assay agrees with the cytotoxicity data described above.

Stability in plasma

To obtain preliminary insights into the behavior of the active cyclometalated complexes **1** and **2** under physiological conditions, we assessed their stability in plasma.[30] As shown from the LC-UV traces in Figure S18 in the Supporting Information, complexes **1** and **2** exhibited no distinct decomposition plasma after 48 h, which suggested that they are stable under physiological conditions. These results also indicate that the intact complexes **1** and **2** were responsible for the anticancer activity.

Cellular uptake and localization

The extent of the cellular uptake was investigated by treating normoxic HeLa cancer cells with the Ru^{II} complexes (2.0 μM) and cisplatin (2.0 μM) for 8 h by using inductively coupled plasma mass spectrometry (ICP-MS). As expected, the results in Figure 2a indicate that the cyclometalation of the Ru^{II} complexes significantly enhances the cellular uptake. The cyclometalated complex **1** is taken up by the HeLa cells 1.2-, 23-, 32-, 2.7-,4.8-, and 2.6-fold more effectively than complexes **2**, **3**, **4**, **5**, **6**, and cisplatin, respectively. Significantly, the 28-fold increase in cellular uptake between complexes **6** and **1** is accompanied by a 207-fold increase in cytotoxicity, indicating that the increase in the cytotoxicity is primarily attributed to an increase in uptake. These results were in agreement with studies in which complex **1**, which is the most lipophilic complex, exhibited the highest uptake. Additionally, the difference in the uptake of complex **1** in HeLa, A549, A549R, and L02 cells between normoxia and hypoxia is also investigated. As revealed in Figure 2b, complex **1** exhibited equally matched accumulation in the three cancer lines cells and there were no obvious differences between normoxia and hypoxia, indicating that complex **1** exhibits high levels of accumulation in hypoxic cancer cells and positive anticancer activity against different types of cancer. However, the amount of Ru in L02 cells is far less than that in the three cancer lines, which implied improved selectivity for cancer therapy.

In addition, the subcellular distribution of complex **1** and cisplatin were studied in normoxic and hypoxic HeLa cells. The cellular ruthenium or platinum concentration was determined

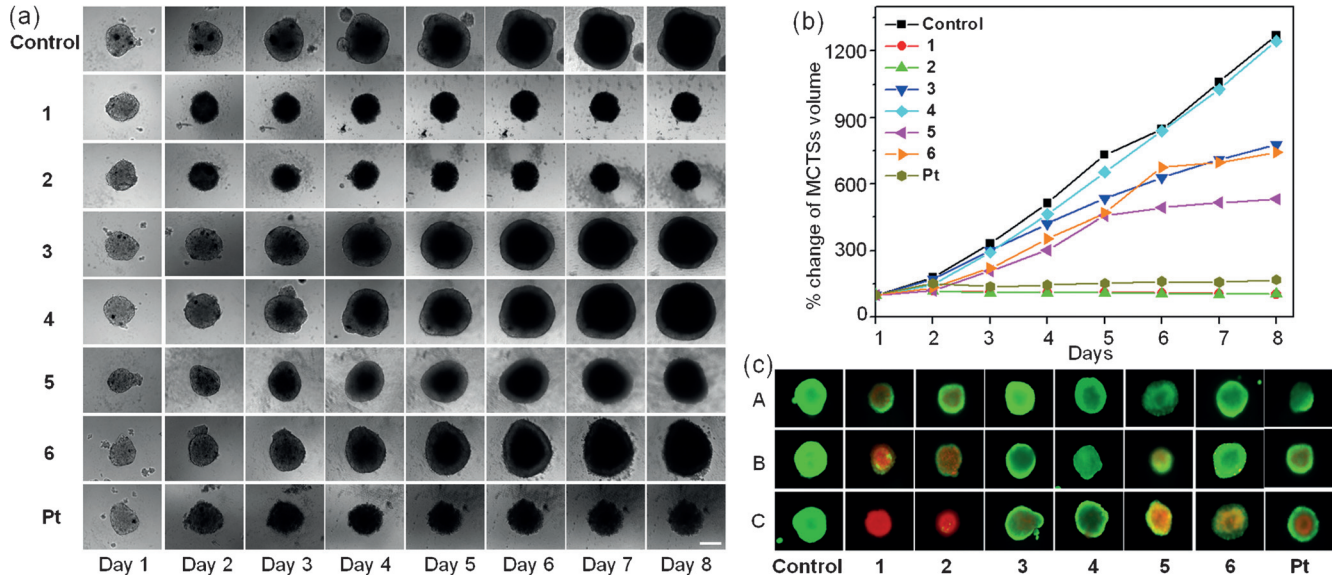

Figure 1. a, b) Growth inhibition of drug-treated HeLa MCTSs of 400 μm diameter by using complexes **1** and **2** (1.0 μM), **3** and **4** (100 μM), **5** and **6** (30 μM), and Pt (60 μM). Scale bar = 300 μm. c) Calcein AM (λ_{ex} = 488, λ_{em} = (550 ± 20) nm) and EthD-1 (λ_{ex} = 488, λ_{em} = (630 ± 20) nm) dual staining of drug-treated HeLa MCTSs: A) complexes **1** and **2** (0.5 μM), **3**–**6**, or Pt (15.0 μM); B) complexes **1** and **2** (1.0 μM), **3**–**6**, or Pt (30.0 μM); and C) complexes **1** and **2** (2.0 μM), **3**–**6**, or Pt (60.0 μM) were incubated with the MCTSs for 48 h.

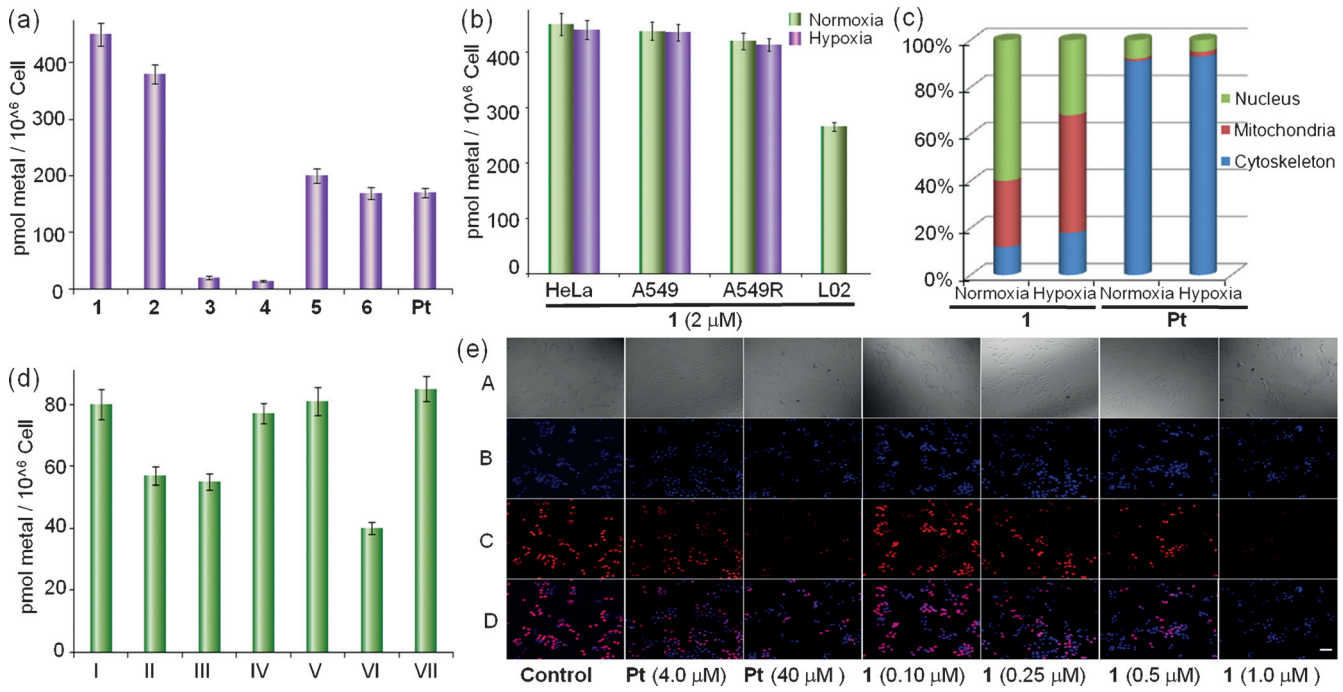

Figure 2. a) Ruthenium uptake in normoxic HeLa cells after exposure to the complexes (2.0 μM) for 8 h. b) Ruthenium uptake in four different normoxic and hypoxic cell lines after exposure to complex **1** (2.0 μM) for 8 h. c) Subcellular distribution of ruthenium and platinum in normoxic and hypoxic HeLa cells after exposure to complex **1** (2.0 μM) and Pt (2.0 μM) for 8 h. d) ICP-MS data for HeLa cells incubated with 2.0 μM of complex **1** in the presence of cell uptake inhibitors: I) control cells at 37 °C, II) cells at 4 °C, III) metabolic inhibitors, IV) 50 μM chloroquine, V) 50 mM NH_4Cl, VI) high K^+-HBSS buffer (170 mM K^+), VII) 50 μM valinomycin (containing 6.0 mM K^+). e) The antiproliferative effects of 12 h drug exposures in hypoxic HeLa cells were verified with an EdU assay: A) bright field, B) Hoechst, C) EdU, and D) overlap. Scale bar = 50 μm.

after 8 h of exposure to complex **1** (2.0 μM) and cisplatin (2.0 μM). Interestingly, there is a visible diversity in the subcellular distribution of complex **1** and cisplatin between the normoxic and hypoxic cells. As shown in Figure 2c, approximately 60.0% of the cellular ruthenium was found in the nuclei and 28% in the mitochondria after 8 h exposure for normoxia; however, the amount of ruthenium accumulated in mitochondria exceeded that in the nuclei (mitochondria 50.0, nuclei 32%) after 8 h exposure for hypoxia. For cisplatin, most of the platinum accumulated in the cytoplasm and 8% of the platinum were found in the nuclei in normoxia, which is similar to the distribution of cisplatin in hypoxia. Therefore, these results suggested that the tumor microenvironment can affect the subcellular distribution of complex **1**, and the nuclei and mitochondria are the main targets of complex **1** both in normoxia and hypoxia, which could provide more insight into the mode of action of complex **1**.

The cellular uptake mechanism of complex **1** in normoxia was further investigated by using ICP-MS. To determine whether complex **1** entered the cell through an energy-dependent or energy-independent transport pathway, HeLa cells were either incubated with this complex at 4 °C or pretreated with the metabolic inhibitors 2-deoxy-D-glucose and oligomycin. Endocytosis is a common, well-known energy-dependent pathway in eukaryotic cells. Therefore, the endocytic inhibitors chloroquine and NH_4Cl were used to examine the role of this pathway in the uptake of complex **1**.[31] Additionally, the cell membrane potential is linked to the cellular uptake. To investigate the effects of the cell membrane potential on the cellular uptake, we reduced the membrane potential by using a high potassium environment (≈170 mM) and increased the membrane potential by using valinomycin. As shown in Figure 2d, there were no significant variations of the uptake in the chloroquine and NH_4Cl groups after treatment with the endocytic inhibitors, suggesting that endocytosis was not responsible for the uptake of complex **1**. The amount of Ru in the groups treated at 4 °C and with the metabolic inhibitors was moderately reduced and significantly decreased in the high K^+ concentration group compared to the control group, which indicated that an energy-dependent pathway and the cell membrane potential are involved in the uptake of complex **1**. This is perhaps not surprising, as cellular uptake is generally complex and diverse.

Antiproliferation assay

Because the cell nuclei are the main targets of complex **1** in hypoxia, we tested the effect of complex **1** on DNA replication. 5-Ethynyl-2′-deoxyuridine (EdU) is a thymidine analogue that can be metabolized by mammalian cells and incorporated into DNA replication, serving as a red fluorescence marker of actively proliferating cells.[32] As shown in Figure 2e, a mass of newly replicated DNA was detected in the nuclei of cells in the control group. Low concentrations of cisplatin (4 μM) induced a very small inhibitory effect on HeLa cells; however, remarkable suppression of the DNA replication could be observed in

the presence of 40 μM cisplatin. For complex **1**, the DNA replication process was distinctly reduced at a concentration of 0.25 μM. At a concentration of 1.0 μM, nearly all DNA synthesis in hypoxic HeLa cells was suppressed. The EdU assay suggested that complex **1** more effectively impeded cellular DNA amplification than cisplatin.

DNA damage

DNA damage is a common physiological phenomenon in cells, and it inhibits DNA replication and induces apoptosis.[33] Moreover, this damage can be detected. The single cell gel is a simple and sensitive method for the detection of DNA damage in an individual eukaryotic cell.[34] ICP-MS analysis proved that the nuclei are the targets of complex **1** in HeLa cancer cells; therefore, the hypoxic HeLa cells were treated with 0.25 mM of complex **1** for 24 h. As shown in Figure 3a, some chromosomal DNA strand breakage was observed, along with the appearance of an obscure "halo" around the nucleus of the HeLa cells. When we expanded to concentrations of 0.5, 1.0, and 2.0 mM of complex **1**, the number of halos were greatly increased. The results demonstrated that the cyclometalated complex **1** could induce DNA damage in HeLa cells at very low concentrations.

Mitochondrial dysfunction

Cancer cells exhibit many adaptive responses to hypoxia, including the optimization of the mitochondrial function.[35] Mitochondrial dysfunction is involved in apoptotic cell death, and the loss of mitochondrial membrane potential (MMP, $\Delta\Psi_m$) is a hallmark of mitochondrial dysfunction.[36] We have found that the mitochondria are the main target of complex **1** in hypoxic HeLa cells, and, consequently, confocal microscopy and flow cytometry were used to confirm whether complex **1** induced apoptosis in hypoxia through mitochondrial damage by using the cationic dye JC-1 as the MMP-sensitive probe.[37] As shown in Figure 3b, the HeLa cells display a significant red-to-green color shift in the presence of complex **1**, indicating the loss of MMP compared with the untreated cells. A concentration-dependent decrease in the red/green fluorescence intensity ratios can be detected, and the representative JC-1 green signals recorded by flow cytometry are shown in Figure 3c. These results indicate that complex **1** induced mitochondrial dysfunction contributes to cellular apoptosis in hypoxia.

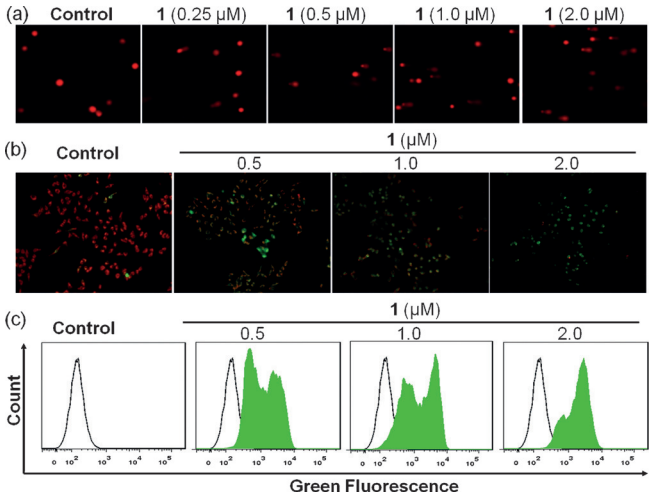

Figure 3. a) Complex **1** induced chromosomal DNA strand breaks in HeLa cells, as detected by the comet assay. b,c) The hypoxic HeLa cells were treated with complex **1** for 24 h and stained with JC-1 to measure the changes in the mitochondrial membrane potential, which were observed under a fluorescence microscope and analyzed by using a flow cytometer.

HIF-1α inhibition

HIF-1α is overexpressed in many cancer cells during hypoxia, and it is connected with HIF-1 activation, oncogene activation, and the loss of tumor suppressor function.[38] The cellular expression of HIF-1α determines the ultimate activation of HIF-1.[39] The cyclometalated complexes exhibit strong toxicity to HeLa cells during hypoxia, which may correlate to HIF-1α inhibition, particularly by complex **1**, the most potent member of the series. Therefore, we determined the effects of this complex on HIF-1α expression in HeLa cells. The Western blot results showed that the complex obviously decreased HIF-1α expression during 24 h of hypoxia (Figure 4). Complex **1** caused a concentration-dependent decrease of HIF-1α expression in HeLa cells, which was also confirmed by immunofluorescence detection (Figure S19 in the Supporting Information). Therefore, this result demonstrates that complex **1** can attenuate HIF-1α expression in HeLa cells, which may contribute to the excellent toxicity of this complex in hypoxic HeLa cells.

Cellular apoptosis

The process of apoptosis is very complex and is regulated by a cascade of proteins, called caspases. Caspase expression is closely related to the hypoxic environment.[40] Therefore, it is important to study the influence of drug-induced cellular apoptosis in hypoxia. Apoptosis is a naturally occurring programmed and targeted cellular death mechanism. Apoptotic cells, however, are transformed into small membrane-bound vesicles (apoptotic bodies) that are engulfed by macrophages in vivo, without an inflammatory response. The harmless removal of cells (e.g., cancer cells) is one consideration in che-

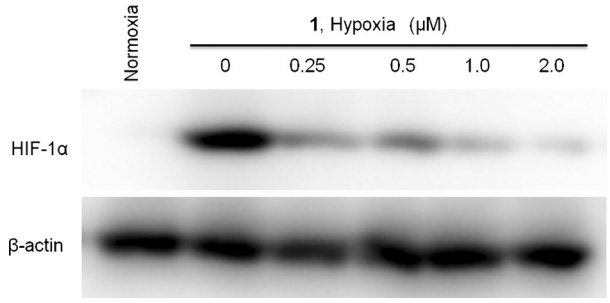

Figure 4. Expression of HIF-1α in HeLa cells after incubation with complex **1** for 24 h.

motherapy.[41] Complex **1** was used to determine whether the inhibitory growth activity of this complex was related to the induction of apoptosis in hypoxia. Therefore, the type of cell death induced by this complex was investigated by apoptosis assays by using (AO/EB) staining.[42] AO is a vital dye that can stain both live and dead cells and shows green fluorescence. EB only stains cells that have lost their membrane integrity and exhibits red fluorescence. Under the fluorescence microscope, the necrotic cells are stained in red but have a nuclear morphology resembling that of viable cells. Apoptotic cells appear green and exhibit morphological changes, such as cell blebbing and the formation of apoptotic bodies. As shown in Figure 5a, the control group shows consistent, live green cells with normal morphology; however, orange apoptotic cells with fragmented chromatin and apoptotic bodies were observed in the cyclometalated complex **1**-treated groups at concentrations of 0.25–1.0 mM after 48 h of incubation, which suggested that low concentrations of complex **1** predominantly induced apoptosis in hypoxic HeLa cells.

Soon after initiating apoptosis, the cells translocate the membrane phosphatidylserine (PS) from the inner face of the plasma membrane to the surface. Once on the cell surface, PS can be easily detected by staining with fluorescently conjugated annexin V, a protein that has a high affinity for PS.[43] Cells that have bound annexin V-FITC will show green staining in the plasma membrane. Cells that have lost their membrane integrity will show red staining (PI) throughout the nuclei and a halo of green staining (FITC) on the cell surface (plasma membrane). Therefore, we can use a flow cytometer to distinguish between at least three different cell types during apoptosis: viable cells (annexin V^- and PI^- negative), early apoptotic cells (annexin V-positive but PI-negative), and necrotic or late apoptotic cells (annexin V- and PI-positive). An annexin V/PI apoptosis kit was used to study the nature of the ruthenium(II) complex **1** induced cell death by using flow cytometry. Hypoxic HeLa cells were treated with complex **1** at concentrations of 0.25, 0.5, and 1.0 mM for 48 h. As shown in Figure 5b, annexin V^+ cells were detected at a concentration as low as 0.25 mM, and the amount of annexin V^+ cells increased with increasing concentrations of complex **1**. A total of 75.5% cells were undergoing early and late apoptosis when the cells were treated with 1.0 mM cyclometalated complex **1**. This pathway suggests that induced cell death occurs mainly through apoptosis.

Study of the structure–activity relationship

Although these six Ru^{II} complexes possess very similar structures, they have different anticancer activities. The lipophilicity of these complexes containing the adtpy ligand is greater than the complexes containing the addpy ligand because the sulfur atom of the addpy ligand is more hydrophilic. We modified the charge number of the complexes by replacing the tpy ligand with the pbpy ligand, and altered the volumes of the ancillary ligand by adding the phenyl ring, which increased the lipophilicity and the cellular uptake of the complexes. In this

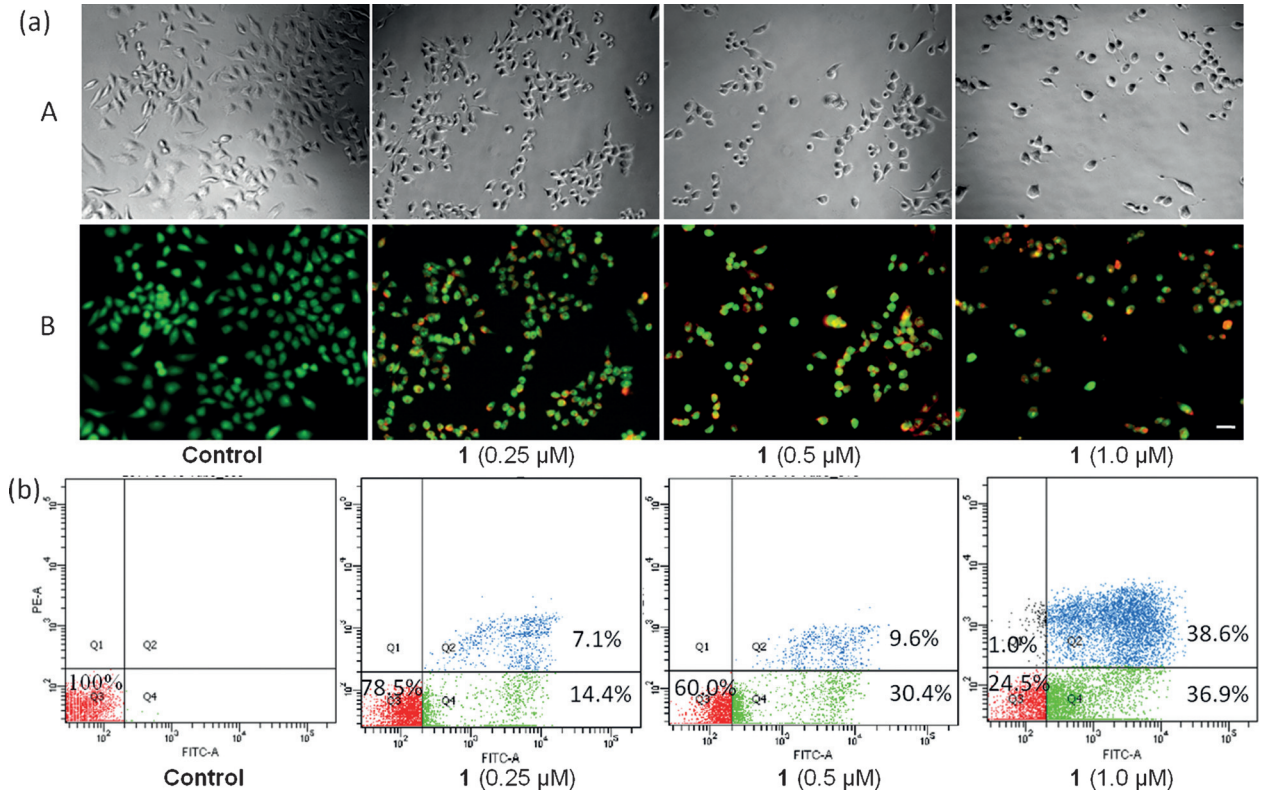

Figure 5. a) Complex **1** treated HeLa cells were stained with AO/EB and observed under a fluorescence microscope, A) bright, B) fluorescent (AO: $\lambda_{ex}=502$, $\lambda_{em}=525$ nm; EB: $\lambda_{ex}=545$, $\lambda_{em}=590$ nm). Scale bar = 50 μm. b) Complex **1** induced apoptotic HeLa cell death as examined by the Annexin V-FITC/PI assay.

study, the lipophilicity, cancer cell toxicity, and cell uptake were distinctly correlated, and followed the order of complex **1** > **2** > **5** > **6** > **3** > **4**. The cyclometalated complexes **1** and **2**, with the valence of +1, are the most lipophilic ones and exhibited the most cellular uptake and the most cytotoxicity. However, complexes **3** and **4**, with a valence of +2, displayed the least lipophilicity, are the least cytotoxic, and exhibited the least cellular uptake. We found that complexes **5** and **6**, with a valence of +2 but with more phenyl rings than complexes **3** and **4**, exhibited moderate lipophilicity and cytotoxicity. Therefore, the cyclometalated complex **1** with the pbpy and adtpy ligands showed the strongest anticancer activity against cancer cells due to good accumulation.

Conclusion

Drug resistance in solid tumors is still a major obstacle for cures and drug discovery; however, hypoxia in solid tumors plays a key role in cellular adaptation and the modulation of gene expression that leads to resistance to chemotherapy and radiotherapy. We demonstrated that the integration of cyclometalated ruthenium(II) complexes with anthraquinone ligands produces compounds that are highly cytotoxic to hypoxic cancer cells. This study showed that the hydrophobicity and cellular uptake properties of the complexes were consistent with their cytotoxicity. The most active drug, that is, complex **1**, accumulates well in HeLa cancer cells, and exhibited 46-fold and 61-fold higher cytotoxic potency than cisplatin in hypoxic cells and 3D multicellular tumor spheroids. Further studies demonstrated that complex **1** preferentially accumulated in the mitochondria of hypoxic HeLa cells, and both the mitochondria and the nuclei are the main targets of complex **1**, which induced apoptosis through multiple synergistic pathways. Complex **1** inhibited DNA replication, promoted DNA damage, and mitochondrial dysfunction, and inhibited HIF-1α in hypoxic HeLa cells, indicating that complex **1** is highly toxic to hypoxic tumor cells. Our results also demonstrated that complex **1** may be a potential therapeutic anticancer candidate for overcoming the resistance to chemotherapy.

Experimental Section

Materials

All reagents were purchased from commercial sources in reagent grade and used as received, unless stated otherwise. The ^{1}H NMR spectra were recorded on a Varian Mercury Plus 300 nuclear magnetic resonance spectrometer at 25 °C. All chemical shifts are reported relative to tetramethylsilane (TMS). The electrospray ionization mass spectra (ESI-MS) were recorded on a LCQ system (Finnigan MAT, USA), and the reported *m/z* values in this work are for the major peaks in the isotope distribution. Microanalysis (C, H, and N) was carried out by using an Elemental Vario EL CHNS analyzer (Germany). The infrared spectra were obtained with a Bruker IFS 113v Fourier transform spectrometer equipped with a global light source and a liquid N_2-cooled mercury cadmium telluride detector. All of the tested complexes were dissolved in DMSO, and the concentration of DMSO was 1% (v/v). The phosphate-buffered saline (PBS) solutions of complexes **1**–**6** were shown to be stable for at least 48 h at room temperature as monitored by UV/Vis spectroscopy before the experiments. Cisplatin, Hoechst 33258, 3-(4,5-dimethylthiazol-2-yl)-2,5-diphenyltetrazolium bromide, JC-1, and propidium iodide (PI) were obtained from Sigma–Aldrich. The annexin V-FITC apoptosis assay kit (Life Technologies, Guangzhou, China) and the 5-ethynyl-2′-deoxyuridine (EdU) labeling/detection kit (Ribobio, Guangzhou, China) were used.

Synthesis and characterization

Synthesis of adtpy: 2-Acetylpyridine (302 mg, 2.5 mmol), KOH (280 mg, 5.0 mmol), and a concentrated aqueous solution of NH_4OH (10 mL) were added to a solution of 2-formyl-9,10-anthracenedione (300 mg, 1.25 mmol) in ethanol (100 mL). The reaction mixture was stirred at ambient temperature for 24 h. The solution was filtered, and a yellow–green precipitate was obtained and washed with water and diethyl ether. Recrystallization from $CHCl_3$/MeOH (2:1, *v/v*) produced a light yellow crystalline solid. Yield: 274 mg, 50%; ^{1}H NMR (300 MHz, $CDCl_3$): $\delta = 8.86$ (s, 2H), 8.82 (d, $J = 1.7$ Hz, 1H), 8.75 (d, $J = 4.0$ Hz, 2H), 8.69 (d, $J = 8.0$ Hz, 2H), 8.46 (d, $J = 8.1$ Hz, 1H), 8.39–8.30 (m, 3H), 7.91 (td, $J = 7.8$, 1.7 Hz, 2H), 7.83 (dd, $J = 5.8$, 3.3 Hz, 2H), 7.39 ppm (dd, $J = 6.5$, 5.7 Hz, 2H); IR (KBr): $\tilde{\nu} = 1681$ cm^{-1} (C=O free); elemental analysis calcd (%) for $C_{29}H_{17}N_3O_2$: C 79.09, H 3.86, N 9.55; found: C 79.21, H 3.98, N 9.36.

Synthesis of addpy: This ligand was synthesized in a similar manner to that described for adtpy, with 2-acetylthiazole (254 mg, 2 mmol) in place of 2-acetylpyridine. Yield: 180 mg, 40%; ^{1}H NMR (300 MHz, $CDCl_3$): $\delta = 8.76$ (d, $J = 2.0$ Hz, 1H), 8.62 (s, 2H), 8.46 (d, $J = 8.1$ Hz, 1H), 8.35 (td, $J = 6.3$, 3.3 Hz, 2H), 8.27 (dd, $J = 8.1$, 1.8 Hz, 1H), 8.01 (d, $J = 3.2$ Hz, 2H), 7.83 (dd, $J = 5.8$, 3.3 Hz, 2H), 7.55 ppm (d, $J = 3.2$ Hz, 2H); IR (KBr): $\tilde{\nu} = 1678$ cm^{-1} (C=O free); elemental analysis calcd (%) for $C_{25}H_{13}N_3O_2S_2$: C 66.52, H 2.88, N 9.55; found: C 66.34, H 3.04, N 9.45.

Synthesis of [Ru(pbpy)(adtpy)](ClO$_4$) (1): By using a previously described procedure, Ru(adtpy)Cl_3 (97 mg, 0.15 mmol) and AgOTf (116 mg, 0.45 mmol) were added to acetone (15 mL), and the mixture was heated to reflux for 3 h. Then, the solution was cooled to room temperature, filtered, and the filtrate was concentrated to dryness in vacuum. A solution of pbpy (35 mg, 0.15 mmol) and DMF (10 mL) was added to the residue, and the mixture was heated to reflux under an argon atmosphere for 24 h. The solution was left to cool to room temperature, the DMF was removed under reduced pressure, and the solid was dissolved in methanol (20 mL). After addition of a saturated aqueous solution of $NaClO_4$, a dark purple precipitate was collected by filtering and washing with water and diethyl ether. The crude product was purified by alumina column chromatography with CH_3CN/toluene (1:1 to 10:1, v/v) as the eluent to afford 100 mg of complex **1** as a purple-black solid (77%). ^{1}H NMR (300 MHz, DMSO): $\delta = 9.46$ (s, 2H), 9.13 (s, 1H), 9.06 (d, $J = 8.1$ Hz, 2H), 8.89 (d, $J = 8.3$ Hz, 1H), 8.72 (dd, $J = 14.7$, 8.0 Hz, 2H), 8.45 (dd, $J = 18.2$, 8.1 Hz, 1H), 8.40 (dd, $J = 18.2$, 8.1 Hz, 1H),8.37–8.25 (m, 2H), 8.17 (t, $J = 8.0$ Hz, 1H), 8.04–7.96 (m, 6H), 7.56 (d, $J = 5.3$ Hz, 1H), 7.39 (d, $J = 5.1$ Hz, 2H), 7.26–7.18 (m, 2H), 7.17–7.09 (m, 1H), 6.69 (t, $J = 7.3$ Hz, 1H), 6.46 (t, $J = 7.2$ Hz, 1H), 5.66 ppm (d, $J = 7.3$ Hz, 1H); IR (KBr): $\tilde{\nu} = 1673$ cm^{-1} (C=O free); MS (ESI): *m/z*: 771.8 $[M-ClO_4]^+$; elemental analysis calcd (%) for $C_{45}H_{28}N_5O_2Ru$: C 61.93, H 3.33, N 8.03; found: C 62.11, H 3.51, N 8.21.

Synthesis of [Ru(pbpy)(addpy)](ClO$_4$) (2): This complex was synthesized in a similar manner to that described for [Ru(pbpy)(adtpy)](ClO_4), with Ru(addpy)Cl_3 (64 mg, 1 mmol) in place of Ru(adtpy)Cl_3. Yield: 50 mg, 57%; ^{1}H NMR (300 MHz, DMSO): $\delta = 9.32$ (s,

2H), 9.08 (d, J=1.8 Hz, 1H), 8.87 (dd, J=8.2, 1.9 Hz, 1H), 8.68 (dd, J=14.3, 8.0 Hz, 2H), 8.45 (d, J=8.2 Hz, 1H), 8.38 (d, J=8.0 Hz, 1H), 8.31 (ddd, J=8.9, 5.7, 3.1 Hz, 2H), 8.17 (t, J=7.9 Hz, 1H), 8.07–7.90 (m, 5H), 7.84 (d, J=7.9 Hz, 1H), 7.47 (d, J=5.2 Hz, 1H), 7.20–7.09 (m, 1H), 6.96 (d, J=3.4 Hz, 2H), 6.69 (t, J=7.5 Hz, 1H), 6.47 (t, J=7.3 Hz, 1H), 5.46 ppm (d, J=7.4 Hz, 1H); IR (KBr): $\tilde{\nu}$=1675 cm^{-1} (C=O free); MS (ESI): m/z: 784.0 $[M-ClO_4]^+$; elemental analysis calcd (%) for $C_{41}H_{24}N_5O_2S_2Ru$: C 55.66, H 2.83, N 7.92; found: C 55.56, H 2.95, N 8.12.

Synthesis of [Ru(tpy)adtpy](ClO$_4$)$_2$ (3): Complex **3** was synthesized according to the previously described procedure for the complex by using tpy (64 mg, 0.27 mmol) and Ru(adtpy)Cl_3 (176 mg, 0.27 mmol) giving a dark-red solid. Yield: 130 mg, 49%; ^{1}H NMR (300 MHz, DMSO): δ=9.65 (s, 2H), 9.23–9.17 (m, 3H), 9.12 (dd, J=8.4, 4.9 Hz, 2H), 8.87 (dd, J=11.8, 6.0 Hz, 3H), 8.59 (dd, J=7.8, 4.8 Hz, 2H), 8.40–8.34 (m, 2H), 8.11 (t, J=4.2 Hz, 2H), 8.06 (dd, J=6.3, 3.9 Hz, 4H), 7.59 (d, J=3.0 Hz, 2H), 7.49 (d, J=3.0 Hz, 2H), 7.35–7.30 (m, 2H), 7.29 ppm (dd, J=4.5, 3.4 Hz, 2H); IR (KBr): $\tilde{\nu}$=1680 cm^{-1} (C=O free); MS (ESI): m/z: 386.9 $[M-2ClO_4]^{2+}$; elemental analysis calcd (%) for $C_{44}H_{28}N_6O_2Ru$: C 54.32, H 2.88, N 8.64; found: C 56.43, H 3.15, N 8.52.

Synthesis of [Ru(tpy)addpy](ClO$_4$)$_2$ (4): Complex **4** was synthesized according to the previously described procedure for the complex by using tpy (64 mg, 0.27 mmol) and Ru(addpy)Cl_3 (179 mg, 0.27 mmol) giving a dark-red solid. Yield: 193 mg, 72%; ^{1}H NMR (300 MHz, DMSO): δ=9.57 (s, 2H), 9.14 (s, 1H), 9.10 (d, J=6.2 Hz, 2H), 8.89 (dd, J=6.2, 2.0 Hz, 1H), 8.83 (d, J=6.0 Hz, 2H), 8.57 (dt, J=6.0, 3.0 Hz, 2H), 8.39–8.32 (m, 2H), 8.11 (d, J=2.6 Hz, 2H), 8.06 (dd, J=6.1, 3.5 Hz, 4H), 7.51 (d, J=4.2 Hz, 2H), 7.32–7.27 (m, 2H), 7.22 ppm (d, J=2.5 Hz, 2H); IR (KBr): $\tilde{\nu}$=1680 cm^{-1} (C=O free); MS (ESI): m/z: 393.1 $[M-2ClO_4]^{2+}$; elemental analysis calcd (%) for $C_{40}H_{24}N_6O_2S_2Ru$: C 48.78, H 2.44, N 8.54; found: C 50.01, H 2.56, N 8.40.

Synthesis of [Ru(bbp)adtpy](ClO$_4$)$_2$ (5): Complex **5** was synthesized according to the previously described procedure for the complex by using bbp (85 mg, 0.27 mmol) and Ru(adtpy)Cl_3 (176 mg, 0.27 mmol) giving a dark-red solid. Yield: 186 mg, 65%; ^{1}H NMR (300 MHz, DMSO): δ=9.71 (s, 2H), 9.31 (s, 1H), 9.14–9.00 (m, 2H), 8.69 (d, J=7.9 Hz, 2H), 8.60–8.52 (m, 2H), 8.35 (dd, J=13.1, 5.6 Hz, 2H), 8.07–7.99 (m, 2H), 7.93 (t, J=7.3 Hz, 3H), 7.58 (d, J=8.2 Hz, 2H), 7.48 (d, J=5.5 Hz, 2H), 7.28–7.20 (m, 2H), 7.12 (t, J=7.2 Hz, 2H), 6.88 (t, J=7.1 Hz, 2H), 6.00 ppm (d, J=7.7 Hz, 2H); IR (KBr): $\tilde{\nu}$=1673 cm^{-1} (C=O free); MS (ESI): m/z: 425.8 $[M-2ClO_4]^{2+}$, 851.3 $[M-2ClO_4-H]^+$; elemental analysis calcd (%) for $C_{48}H_{30}N_8O_2Ru$: C 54.86, H 2.86, N 8.54; found: C 55.01, H 2.72, N 8.43.

Synthesis of [Ru(bbp)addpy](ClO$_4$)$_2$ (6): Complex **6** was synthesized according to the previously described procedure for the complex by using bbp (85 mg, 0.27 mmol) and Ru(addpy)Cl_3 (179 mg, 0.27 mmol) giving a dark-red solid. Yield: 170 mg, 60%; ^{1}H NMR (300 MHz, DMSO): δ=9.61 (s, 2H), 9.27 (s, 1H), 9.03 (d, J=9.4 Hz, 1H), 8.70 (d, J=7.9 Hz, 2H), 8.63–8.51 (m, 2H), 8.35 (dd, J=12.0, 3.5 Hz, 2H), 8.08–7.99 (m, 4H), 7.62 (d, J=8.1 Hz, 2H), 7.27–7.14 (m, 4H), 6.95 (t, J=7.2 Hz, 2H), 6.01 ppm (d, J=8.9 Hz, 2H); IR (KBr): $\tilde{\nu}$=1672 cm^{-1} (C=O free); MS (ESI): m/z: 431.5 $[M-2ClO_4]^{2+}$, 863.2 $[M-2ClO_4-H]^+$; elemental analysis calcd (%) for $C_{44}H_{26}N_8O_2S_2Ru$: C 49.72, H 2.45, N 10.55; found: C 49.62, H 2.63, N 10.78.

Cell lines and culture conditions

The HeLa human cervical carcinoma cell line, the A549 and A549R lung carcinoma cell lines, and the L02 human hepatocyte cell line were obtained from the Experimental Animal Center of Sun Yat-Sen University (Guangzhou, China). The cells were maintained in DMEM (Dulbecco's modified Eagle's medium, Gibco BRL) or RPMI 1640 (Roswell Park Memorial Institute 1640, Gibco BRL) medium supplemented with 10% FBS (fetal bovine serum, Gibco BRL), streptomycin (100 mg mL^{-1}) and penicillin (100 U mL^{-1}) (Gibco BRL) in a humidified incubator at 37 °C with 5% CO_2. The hypoxic culture conditions are similar to the normoxic conditions, with 1% O_2 in place of 20% O_2, and the concentration of oxygen is adjusted through the ventilation with high-purity nitrogen gas in an incubator.

Cellular accumulation studies

The cells were plated at a density of 1×10^5 cells mL^{-1} in DMEM medium (10 mL) of for 24 h at 37 °C with 5% CO_2 under hypoxic or normoxic conditions. The ruthenium complexes (2.0 mM) or cisplatin (2.0 mM) were added to the culture medium and incubated for 8 h, and removed with a cold PBS and trypsin/ethylenediaminetetraacetic acid (EDTA) solution into a centrifuge tube for counting. Then, the nuclear and cytoplasm fractions of the HeLa cells were extracted by using a nuclear and cytoplasmic protein extraction kit. The samples were digested overnight in 20% HNO_3 and 10% H_2O_2 at room temperature. Each sample was then diluted with Milli-Q water to obtain a 2% HNO_3 sample solution. The ruthenium or platinum content was determined by using an inductively coupled plasma mass spectrometer (ICP-MS Thermo Elemental Co., Ltd.).

Distribution coefficient of Ru

The distribution coefficients ($\log P_{o/w}$) were determined by liquid–liquid extraction between *n*-octanol (oil) and phosphate buffer (0.2 M, pH 7.4) with the flask-shaking method. *n*-Octanol and the phosphate buffer were mutually saturated with each other for at least 12 h before use. An aliquot of the ruthenium complex stock solution was added to the phosphate buffer at concentrations <10 mg mL^{-1}, and the mixture was shaken at 80 rpm for one day to allow adequate partitioning at 37 °C. After the sample was centrifuged at 3000 rpm for 10 min, the aqueous layer was used for the ruthenium analysis, and the Ru content in the aqueous layer was then measured by ICP-MS and used to calculate the $\log P_{o/w}$ values.

Stability in human plasma

The stability of complexes **1**, **2**, and PZQ in plasma was assessed by using a procedure analogous to a recently reported method.[17d] Aliquots (12.5 μL) of a Ru complex solution and of a diazepam solution (12.5 μL) were added to the plasma (975 μL). The resulting mixture was incubated for 48 h at 37 °C with continuous and gentle shaking (≈300 rpm). The reaction was stopped by the addition of acetonitrile (4 mL), and the mixture was centrifuged for 10 min at 2000 *g* at 4 °C. The acetonitrile was evaporated, and the residue was suspended in CH_3CN/H_2O (3:1, v/v; 100 mL). The filtrate was analyzed by HPLC-UV spectroscopy. An aliquot of the solution (100μL) was injected into an HPLC system (Thermo, USA) connected to a UV/Vis spectrophotometer. A Hypersil Gold Dim (100×2.1 mm, Thermo, USA) reversed-phase column was used at a flow rate of 0.5 mL min^{-1}. The runs were performed with a linear gradient of A (acetonitrile; Sigma–Aldrich, HPLC grade) in B (distilled water containing 0.02% trifluoroacetic acid (TFA) and 0.05% HCOOH).

Cytotoxicity test on a 2D cancer cell monolayer

The cytotoxicity of the ruthenium complexes were determined by the MTT assay. Briefly, the cells were seeded into 96-well microtiter plates at (1×10^4 cells per well), and grown overnight at 37 °C in a 5% CO_2 incubator under normoxic or hypoxic conditions, and different concentrations of the complexes were added to the culture media. The plates were then incubated for 48 h under the same conditions. The stock MTT dye solution (20 μL, 5 mg mL^{-1}) was added to each well. After 4 h of incubation, the cultures were removed and DMSO (150 μL) was added to each well. The optical density of each well was measured on a microplate spectrophotometer at a wavelength of $\lambda = 595$ nm.

Cytotoxicity test on MCTSs

HeLa MCTSs (diameter ≈400 mm) were treated by carefully replacing 50% of the medium with drug-supplemented standard medium by using an eight-channel pipette. In parallel, 50% of the solvent-containing medium were replaced by solvent-free medium for the untreated MCTSs. Three MCTSs were treated per condition and drug concentration, and the DMSO volume was less than 1% (v/v). The MCTSs were then allowed to incubate for another 48 h. The cytotoxicity of the ruthenium complexes toward the MCTSs was measured by the adenosine triphosphate (ATP) concentration with the Cell TiterGlo kit (Promega). After 30 min of incubation, the MCTSs were carefully transferred into black-sided, flat-bottomed 96-well plates (Corning) and mixed with a pipette for luminescence measurements on an Infinite M200 PRO equipment (TECAN).

Real-time cell growth and proliferation assay

This experiment was carried out by using an xCELLigence RTCA DP system real-time cell analyzer (Roche Diagnostics GmbH, Germany), which was placed in a humidified incubator maintained at 37 °C with 5% CO_2 and 20 or 1% O_2. Growth curves were constructed by using 16-well plates (E-plate 16, Roche Diagnostics GmbH, Germany). To quantify the cell status based on the measured cell electrode impedance, the parameter cell index (CI) is derived according to $CI = \max_{i=1,\ldots,N}(R_{cell}(i)/R_b(i)1)$, where $R_{cell}(i)$ and $R_b(i)$ are the frequency-dependent electrode resistances (a component of impedance) in the presence or absence of cells, respectively; N is the number of the frequency points at which the impedance is measured. CI is a relative value to indicate how many cells are attached to the electrodes. The slope of the CI curve reflects the growth speed of the cells. In brief, an aliquot of the cell culture medium (80 mL) was added into each well of E-plate 16 and then the E-plate 16 was connected to the system and checked for proper electrical contacts; the background impedance was also measured after 30 s. Meanwhile, the HeLa cells were re-suspended into the cell culture medium and adjusted to 5×10^4 cells mL^{-1}. Portions of each cell suspension (100 mL) were added onto the wells of the E-plate 16. Approximately 18 h after seeding, complex **1** (0.25, 0.5, or 1.0 mM) was added and the cells were automatically monitored over 60 h by the xCELLigence system. Data analysis was conducted by using the RTCA software, version 1.2, supplied with the instrument.

Live/dead viability/cytotoxicity assay in the MCTSs

The live/dead assay in the MCTSs was performed by using the LIVE/DEAD viability/cytotoxicity kit for mammalian cells (Life Technologies). Live cells in the MCTSs were distinguished by the presence of ubiquitous intracellular esterase activity, as determined by the enzymatic conversion of the virtually non-fluorescent, cell-permeable calcein AM to the intensely fluorescent calcein ($\lambda_{ex} = 495$, $\lambda_{em} = 515$ nm). EthD-1 would enter the cells with damaged membranes and undergo a 40-fold enhancement of the fluorescence upon binding to nucleic acids, thereby producing a bright red fluorescence in the dead cells ($\lambda_{ex} = 495$, $\lambda_{em} = 635$ nm). EthD-1 is excluded by the intact plasma membrane of live cells. The determination of the cell viability depends on these physical and biochemical cell properties. After treatment with the ruthenium complexes, each MCTS was incubated with a solution (10 μL) of calcein AM (2 mM) and EthD-1 (4 mM) for 40 min at room temperature in the dark and imaged directly by using an inverted fluorescence microscope (Zeiss Axio Observer D1, Germany).

Western blot analysis

The HeLa cells were seeded into 100 mm tissue culture dishes (Corning), incubated for 24 h, and then treated with complex **1** for 24 h. The cells were washed with ice-cold PBS and lysed by incubation in radio immune precipitation assay buffer (RIPA) and a protease inhibitor cocktail (Sigma) for 30 min on ice. The lysates were centrifuged at 15000 rpm for 15 min at 4 °C, and the protein concentrations were quantified by a BCA protein assay reagent kit (Novagen Inc, USA). The proteins were separated on precast NuPAGE 4 to 12% polyacrylamide gradient Bis-Tris gels (Invitrogen) under denaturing conditions, transferred to PVDF membranes (Invitrogen), and subjected to Western blot analysis. Mouse monoclonal anti-HIF-1α (Proteintech USA) and rabbit anti-β-actin (Cell Signaling Technology, USA) antibodies were diluted (1:300 and 1:2000, respectively) in PBS containing 5% nonfat powdered milk and 0.1% Tween-20 and then incubated with the membrane overnight at 4 °C. Horseradish peroxidase conjugated secondary antibodies (Cell Signaling) were used. The bound immune complexes were detected by using an ECL prime Western blot detection reagent (Amersham Inc., USA). The images were captured on FluorChem M (ProteinSimple, Santa Clara, CA).

Fluorescent antibody technique

The cells were seeded into 96-well microtiter plates, grown overnight at 37 °C in a 5% CO_2 and 1% O_2, and different concentrations of complex **1** were added to the culture media. The plates were incubated for 24 h, and then the cultures were removed. Afterwards, the cultured HeLa cells were fixed with 4% paraformaldehyde (pH 7.4) for 30 min. Next, the cells were washed with PBS three times and blocked with 1× PBS-1% BSA-4% goat serum (50 mL) for 1 h. Then, the samples were washed thrice with PBS (100 mL) for 5 min each and stained with primary antibody overnight. After washing five times with 1×PBS-0.2% BSA for 5 min each, the sample was stained with the fluorescently conjugated secondary antibody for 60 min at RT in PBS-1% BSA (40 mL). Following washes with 0.5% TritonX-100 in PBS, PBS (100 mL) was added into each well for observation under an inverted fluorescence microscope (Zeiss Axio Observer D1).

Alexa Fluors488 annexin V/PI double staining

HeLa cells were plated at 5×10^5 cells per well in a 6-well plate with various concentrations (0.25, 0.5, or 1.0 mM) of complex **1** and were incubated in for 48 h under hypoxic conditions. The cells were centrifuged, washed twice with cold PBS, and re-suspended in the binding buffer (0.5 mL) from the Annexin V/PI apoptosis Kit (MultiSciences (Lianke) Biotech Co., Ltd.). Then, Annexin V-FITC (5 mL) and PI (10 mL) were added into the sample solution. After

incubation for 5 min in the dark, the specimens were quantified by flow cytometry on a FACS Canto II (BD Biosciences, USA).

EdU assay

EdU is a type of thymine nucleoside analogue, which is a new type of nucleoside markers that can replace thymine (T) during DNA replication in synthetic DNA molecules. After a cell cycle of EdU incubation, EdU will enter all the cells, to achieve the aim of EdU-labeled cells by using the 5-ethynyl-2′-deoxyuridine (EdU)-labeling/detection kit (Ribobio, Guangzhou, China). Briefly, HeLa cells were seeded into 96-well microtiter plates at 1×10^4 cells per well and grown overnight at 37 °C under hypoxic conditions. Different concentrations of complex **1** or cisplatin were added to the culture media and incubated for 12 h. The EdU (100 μL, 10 μM EdU) solution was then added to each well, incubated for 24 h at 37 °C, and the cultures were then removed. Afterwards, the cultured cells were fixed with 4% paraformaldehyde (pH 7.4) for 30 min and incubated with glycine (50 mL 2 mg mL^{-1}) for 5 min. After washing with PBS twice, each well was stained with the anti-EdU working solution (100 mL) at room temperature for 30 min on the table concentrator. Following washes with 0.5% TritonX-100 in PBS, the cells were incubated with the Hoechst 33342 dye at room temperature on the table concentrator. After incubation for 0.5 h, the staining reaction liquid was abandoned and PBS (100 mL) was added into each well for observation under a confocal laser scanning microscope (TCS SP2, Leica Microsystems, Germany).

Cell uptake mechanism

The cells treated with the inhibitors and complex **1** were washed, and the extent of uptake was analyzed by ICP-MS. The cells were incubated with complex **1** (2.0 μM) for 1 h at 37 °C as the control. For metabolic inhibition, the cells were incubated with complex **1** (2.0 μM) for 1 h at 4 °C for ICP-MS analysis or treated with 2-deoxy-D-glucose (50 mM) and oligomycin (5 μM) in PBS for 1 h at 37 °C. The cells were then rinsed and suspended in PBS and the cells were incubated with complex **1** (2.0 μM) for 1 h at 37 °C. For endocytic inhibition, the HeLa cells were detached from the culture and pre-incubated with NH_4Cl (50 mM) or chloroquine (100 μM) in PBS for 1 h at 37 °C. The cells were then washed with PBS and incubated with complex **1** (2.0 μM) for 1 h at 37 °C for ICP-MS analysis. For modulation of the membrane potential, the HeLa cells were detached from the culture and washed with either high K^+-HBSS (containing 170 mM K^+) or HBSS (containing 5.8 mM K^+). The cells in HBSS were pretreated with valinomycin (50 μM) for 30 min at 37 °C. The cells were incubated with complex **1** (2.0 μM) for 1 h at 37 °C in either high K^+-HBSS (to depolarize the cells) or valinomycin (to hyperpolarize the cells) for ICP-MS analysis.

Fragmentation of nuclear DNA by the comet assay

An alkaline single-cell gel electrophoresis (comet assay) was performed to investigate the extent of DNA damage induced by various concentrations of complex **1** (0.25, 0.5, 1.0, or 2.0 mM) in hypoxic HeLa cells. Briefly, 10000 cells per mL of the untreated controls or the treated HeLa cells were mixed with 0.8% low-melting-point agarose at a ratio of 1:10 (v/v), and then the mixtures were spread on slides precoated with 1% normal-melting agarose. The slides were placed in the dark at 0 °C for 15 min and then lysed in a precooled lytic solution (2.5 M NaCl, 10 mM Tris base, 100 mM EDTA, 1% TritonX-100, and 10% DMSO, pH 10) at 4 °C for 2 h in the dark. Next, the slides were washed and equilibrated by using a precooled alkaline electrophoresis buffer (0.3 M NaOH and 1 mM EDTA, pH 13). The slides were electrophoresed at 20 V and 300 mA in the precooled alkaline electrophoresis buffer for 20 min, and then washed and neutralized with 0.4 M Tris-HCl (pH 7.5). The slides were fixed in a 70% ethanol solution for 5 min, stained with ethidium bromide (EB) solution (2 mg mL^{-1}) for 10 min in the dark, and analyzed by an inverted fluorescence microscope (Zeiss Axio Observer D1).

Induction of mitochondrial dysfunction

HeLa cells were cultured in 6-well tissue culture plates for 24 h and then treated with complex **1** (0.5, 1.0, or 2.0 mM) for 24 h under hypoxic conditions. After the treatment, the cells were collected and re-suspended to a final concentration of 1×10^6 cells mL^{-1} in the pre-warmed staining working solution containing JC-1 (5 μg mL^{-1}), and then incubated for 15 min at 37 °C. Subsequently, the cells were washed twice with pre-warmed PBS and analyzed immediately on a FACS Canto II flow cytometer (BD Biosciences, USA). The mean red and green fluorescence intensities were analyzed by using Tree Star (OR, USA); 10000 events were acquired for each sample.

Acknowledgements

This work was supported by the 973 program (No. 2015CB856301), the National Science Foundation of China (Nos. 21172273, 21171177, 21471164, and J1103305), and the Program for Changjiang Scholars and Innovative Research Team in University of China (No. IRT1298).

Keywords: anthraquinones · cyclometalation · cytotoxicity · hypoxia · ruthenium

[1] T. Henning, M. Kraus, M. Brischwein, A. M. Otto, B. Wolf, *Anti-Cancer Drugs* **2004**, *15*, 7 – 14.

[2] a) J. Chiche, M. C. Brahimi-Horn, J. Pouysségur, *J. Cell. Mol. Med.* **2010**, *14*, 771 – 794; b) F. Perche, S. Biswas, T. Wang, L. Zhu, V. Torchilin, *Angew. Chem. Int. Ed.* **2014**, *53*, 3362 – 3366; *Angew. Chem.* **2014**, *126*, 3430 – 3434.

[3] J. Wang, Z. Lu, Y. Gao, M. G. Wientjes, J. L. Au, *Nanomedicine* **2011**, *6*, 1605 – 1620.

[4] R. Cairns, I. Papandreou, N. Denko, *Mol. Cancer Res.* **2006**, *4*, 61 – 70.

[5] A. Wouters, B. Pauwels, F. Lardon, J. B. Vermorken, *Oncologist* **2007**, *12*, 690 – 712.

[6] a) M. Koritzinsky, B. G. Wouters, Ø. Åmellem, E. O. Pettersen, *Int. J. Radiat. Oncol. Biol. Phys.* **2001**, *77*, 319 – 328; b) Y.-L. Hu, M. DeLay, A. Jahangiri, A. M. Molinaro, S. D. Rose, W. S. Carbonell, M. K. Aghi, *Cancer Res.* **2012**, *72*, 1773 – 1783.

[7] a) F. Zölzer, C. Streffer, *Int. J. Radiat. Oncol. Biol. Phys.* **2002**, *54*, 910 – 920; b) J. Pouysségur, F. Dayan, N. M. Mazure, *Nature* **2006**, *441*, 437 – 443; c) J. C. Knight, M. Wuest, F. A. Saad, M. Wang, D. W. Chapman, H.-S. Jans, S. E. Lapi, B. M. Kariuki, A. J. Amoroso, F. Wuest, *Dalton Trans.* **2013**, *42*, 12005 – 12014.

[8] a) K. L. Bennewith, S. Dedhar, *BMC Cancer* **2011**, *11*, 504; b) P. Carmeliet, Y. Dor, J.-M. Herbert, D. Fukumura, K. Brusselmans, M. Dewerchin, M. Neeman, F. Bono, R. Abramovitch, P. Maxwell, *Nature* **1998**, *394*, 485 – 490; c) J. Bryant, S. Meredith, K. Williams, A. White, *Lung Cancer* **2014**, *86*, 126 – 132.

[9] a) G. L. Semenza, *Nat. Rev. Cancer* **2003**, *3*, 721 – 732; b) Y. Hu, J. Liu, H. Huang, *J. Cell. Biochem.* **2013**, *114*, 498 – 509.

[10] a) L. H. Patterson, *Cancer Metastasis Rev.* **1993**, *12*, 119 – 134; b) S. Danson, T. H. Ward, J. Butler, M. Ranson, *Cancer Treat. Rev.* **2004**, *30*, 437 – 449.

[11] a) M.-K. Ha, Y. H. Song, S.-J. Jeong, H.-J. Lee, J. H. Jung, B. Kim, H. S. Song, J.-E. Huh, S.-H. Kim, *Biol. Pharm. Bull.* **2011**, *34*, 1432 – 1437; b) Q.

Huang, G. Lu, H.-M. Sben, M. C. M. Cbung, C. N. Ong, *Med. Res. Rev.* **2007**, *27*, 609 – 630.
[12] A. Liwo, D. Jeziorek, T. Ossowski, D. Dyl, A. Tempczyk, J. Tarasiuk, M. N. E. Borowski, W. Woznicki, *Acta Biochim. Pol.* **1995**, *42*, 445 – 456.
[13] a) D. Shrimali, M. K. Shanmugam, A. P. Kumar, J. Zhang, B. K. H. Tan, K. S. Ahn, G. Sethi, *Cancer Lett.* **2013**, *341*, 139 – 149; b) M. H. El-Dakdouki, N. Adamski, L. Foster, M. P. Hacker, P. W. Erhardt, *J. Med. Chem.* **2011**, *54*, 8224 – 8227; c) J. J. Newsome, M. Hassani, E. Swann, J. M. Bibby, H. D. Beall, C. J. Moody, *Bioorg. Med. Chem.* **2013**, *21*, 2999 – 3009.
[14] L. L. Silver, *Nat. Rev. Drug Discovery* **2007**, *6*, 41 – 55.
[15] a) G. S. Yellol, A. Donaire, J. G. Yellol, V. Vasylyeva, C. Janiak, J. Ruiz, *Chem. Commun.* **2013**, *49*, 11533 – 11535; b) R. R. Ye, C. P. Tan, L. He, M. H. Chen, L. N. Ji, Z. W. Mao, *Chem. Commun.* **2014**, *50*, 10945 – 10948; c) D. Griffith, J. P. Parker, C. J. Marmion, *Anti-Cancer Agents Med. Chem.* **2010**, *10*, 354 – 370; d) Z. Z. Zhu, X. Y. Wang, T. J. Li, S. Aime, P. J. Sadler, Z. J. Guo, *Angew. Chem. Int. Ed.* **2014**, *53*, 13225 – 13228; *Angew. Chem.* **2014**, *126*, 13441 – 13444; e) D.-L. Ma, V. P.-Y. Ma, D. S.-H. Chan, K.-H. Leung, H.-Z. He, C.-H. Leung, *Coord. Chem. Rev.* **2012**, *256*, 3087 – 3113; <lit f> Z. Liu, P. J. Sadler, *Acc. Chem. Res.* **2014**, *47*, 1174 – 1185.
[16] a) C. Qian, J. Q. Wang, C. L. Song, L. L. Wang, L. N. Ji, H. Chao, *Metallomics* **2013**, *5*, 844 – 854; b) J. F. Kou, C. Qian, J. Q. Wang, X. Chen, L. L. Wang, H. Chao, L. N. Ji, *J. Biol. Inorg. Chem.* **2012**, *17*, 81 – 96.
[17] a) L. Fetzer, B. Boff, M. Ali, X. Meng, J.-P. Collin, C. Sirlin, C. Gaiddon, M. Pfeffer, *Dalton Trans.* **2011**, *40*, 8869 – 8878; b) J.-P. Djukic, J.-B. Sortais, L. Barloy, M. Pfeffer, *Eur. J. Inorg. Chem.* **2009**, 817 – 853; c) H. Huang, P. Zhang, H. Chen, L. Ji, H. Chao, *Chem. Eur. J.* **2015**, *21*, 715 – 725; d) H. Huang, P. Zhang, B. Yu, Y. Chen, J. Wang, L. Ji, H. Chao, *J. Med. Chem.* **2014**, *57*, 8971 – 8983.
[18] F. Pampaloni, E. G. Reynaud, E. H. K. Stelzer, *Nat. Immunol.* **2007**, *8*, 839 – 845.
[19] M. Jäger, L. Eriksson, J. Bergquist, O. Johansson, *J. Org. Chem.* **2007**, *72*, 10227 – 10230.
[20] P. G. Bomben, K. C. D. Robson, P. A. Sedach, C. P. Berlinguette, *Inorg. Chem.* **2009**, *48*, 9631 – 9643.
[21] E. C. Constable, M. J. Hannon, *Inorg. Chim. Acta* **1993**, *211*, 101 – 110.
[22] D. Ayres, L. Pinto, S. Giorgio, *J. Parasitol.* **2008**, *94*, 1415 – 1417.
[23] M. Höckel, K. Schlenger, B. Aral, M. Mitze, U. Schäffer, P. Vaupel, *Cancer Res.* **1996**, *56*, 4509 – 4515.
[24] Y. A. Abassi, B. Xi, W. Zhang, P. Ye, S. L. Kirstein, M. R. Gaylord, S. C. Feinstein, X. Wang, X. Xu, *Chem. Biol.* **2009**, *16*, 712 – 723.
[25] a) P. A. Netti, D. A. Berk, M. A. Swartz, A. J. Grodzinsky, R. K. Jain, *Cancer Res.* **2000**, *60*, 2497 – 2503; b) A. Pluen, Y. Boucher, S. Ramanujan, T. D. McKee, T. Gohongi, E. di Tomaso, E. B. Brown, Y. Izumi, R. B. Campbell, D. A. Berk, *Proc. Natl. Acad. Sci. USA* **2001**, *98*, 4628 – 4633.
[26] O. Trédan, C. M. Galmarini, K. Patel, I. F. Tannock, *J. Natl. Cancer Inst.* **2007**, *99*, 1441 – 1454.
[27] a) W. Xin, Z. Xu, W. Jing, Z. Jialiang, W. Wei, J. Xiqun, *Biomaterials* **2013**, *34*, 4667 – 4679; b) J. L. Horning, S. K. Sahoo, S. Vijayaraghavalu, S. Dimitrijevic, J. K. Vasir, T. K. Jain, A. K. Panda, V. Labhasetwar, *Mol. Pharm.* **2008**, *5*, 849 – 862.
[28] J. Friedrich, C. Seidel, R. Ebner, L. A. Kunz-Schughart, *Nat. Protoc.* **2009**, *4*, 309 – 324.
[29] L. Yu, M. C. Chen, K. C. Cheung, *Lab Chip* **2010**, *10*, 2424 – 2432.
[30] M. Patra, K. Ingram, V. Pierroz, S. Ferrari, B. Spingler, J. Keiser, G. Gasser, *J. Med. Chem.* **2012**, *55*, 8790 – 8798.
[31] C. Y. Li, M. X. Yu, Y. Sun, Y. Q. Wu, C. H. Huang, F. Y. Li, *J. Am. Chem. Soc.* **2011**, *133*, 11231 – 11239.
[32] Q. He, L. Man, Y. Ji, F. Ding, *Neurosci. Lett.* **2012**, *521*, 57 – 61.
[33] a) A. Strasser, A. W. Harris, T. Jacks, S. Cory, *Cell* **1994**, *79*, 329 – 339; b) W. P. Roos, B. Kaina, *Trends Mol. Med.* **2006**, *12*, 440 – 450.
[34] V. McKelvey-Martin, M. Green, P. Schmezer, B. Pool-Zobel, M. De Meo, A. Collins, *Mutat. Res.* **1993**, *288*, 47 – 63.
[35] a) N. Chandel, E. Maltepe, E. Goldwasser, C. Mathieu, M. Simon, P. Schumacker, *Proc. Natl. Acad. Sci. USA* **1998**, *95*, 11715 – 11720; b) R.-H. Xu, H. Pelicano, Y. Zhou, J. S. Carew, L. Feng, K. N. Bhalla, M. J. Keating, P. Huang, *Cancer Res.* **2005**, *65*, 613 – 621.
[36] a) L. F. Yousif, K. M. Stewart, S. O. Kelley, *ChemBioChem* **2009**, *10*, 1939 – 1950; b) M. O. Hengartner, *Nature* **2000**, *407*, 770 – 776; c) X. Wang, *Genes Dev.* **2001**, *15*, 2922 – 2933.
[37] S. T. Smiley, M. Reers, C. Mottola-Hartshorn, M. Lin, A. Chen, T. W. Smith, G. Steele, L. B. Chen, *Proc. Natl. Acad. Sci. USA* **1991**, *88*, 3671 – 3675.
[38] a) R. S. Freeman, M. C. Barone, *Curr. Drug Targets: CNS Neurol. Disord.* **2005**, *4*, 85 – 92; b) K. M. Block, H. Wang, L. Z. Szabo, N. W. Polaske, L. K. Henchey, R. Dubey, S. Kushal, C. F. Laszlo, J. Makhoul, Z. Song, *J. Am. Chem. Soc.* **2009**, *131*, 18078 – 18088.
[39] J. I. Bárdos, M. Ashcroft, *Bioessays* **2004**, *26*, 262 – 269.
[40] P. Saikumar, Z. Dong, Y. Patel, K. Hall, U. Hopfer, J. M. Weinberg, M. Venkatachalam, *Oncogene* **1999**, *17*, 3401 – 3415.
[41] X. W. Meng, S.-H. Lee, S. H. Kaufmann, *Curr. Opin. Cell Biol.* **2006**, *18*, 668 – 676.
[42] F. Vartdal, G. Gaudernack, S. Funderud, A. Bratlie, T. Lea, J. Ugelstad, E. Thorsby, *Tissue Antigens* **1986**, *28*, 301 – 312.
[43] I. Vermes, C. Haanen, H. Steffens-Nakken, C. Reutellingsperger, *J. Immunol. Methods* **1995**, *184*, 39 – 51.

Received: June 2, 2015
Published online on September 4, 2015

